Some Remarks on the Effect of Interphases on the Mechanical Response and Stability of Fiber-Reinforced Elastomers

Some remarks on the effect of interphases on the mechanical response and stability of fiber-reinforced elastomers

Katia Bertoldi[a], Oscar Lopez-Pamies[b]

[a] *School of Engineering and Applied Sciences, Harvard University, Cambridge, MA 02138, USA*

[b] *Department of Civil and Environmental Engineering, University of Illinois, Urbana-Champaign, IL 61801-2352, USA*

Abstract

In filled elastomers, the mechanical behavior of the material surrounding the fillers — termed interphasial material — can be significantly different (softer or stiffer) from the bulk behavior of the elastomeric matrix. In this paper, motivated by recent experiments, we study the effect that such interphases can have on the mechanical response and stability of fiber-reinforced elastomers at large deformations. We work out in particular analytical solutions for the overall response and onset of microscopic and macroscopic instabilities in axially stretched 2D fiber-reinforced non-linear elastic solids. These solutions generalize the classical results of Rosen (1965) and Triantafyllidis and Maker (1985) for materials without interphases. It is found that while the presence of interphases does not significantly affect the overall axial response of fiber-reinforced materials, it can have a drastic effect on their stability.

Key words: Finite strain; Microstructures; Homogenization; Instabilities; Bound rubber

1. Introduction

It is by now well established that the portion of material surrounding the fillers in filled elastomers — often referred to as "bound rubber" or more generally as interphasial material — can exhibit a mechanical behavior markedly different (softer or stiffer) from that of the matrix in the bulk. In the case when the surfaces of the fillers are suitably treated to form strong bonds with the matrix, such interphases can be up to one order of magnitude stiffer than the matrix material in the small-deformation regime (see, e.g., [1, 2] and references therein), and possibly even more at large deformations [3]. On the other hand, for untreated surfaces or surfaces that are treated unfavorably to form bonds with the matrix, the interphases can be significantly softer [4].

The study of the chemistry, geometry, and physical properties of interphases in filled elastomers has a long and motley history, yet numerous practical and theoretical issues remain unresolved [5, 6, 7]. From a mechanical point of view, significant effort has been devoted to incorporate interphasial effects in constitutive models, but almost exclusively within the limited context of *small-strain linear elasticity* (see, e.g., [8, 9]). In this paper we investigate the effects that interphases can have on the macroscopic response and stability of filled elastomer at *large deformations*. Motivated by recent experiments [4], and for the sake of relative simplicity, attention is focused on axially stretched fiber-reinforced elastomers consisting of a matrix phase reinforced by a single family of aligned long fibers.

To treat the problem analytically, fiber-reinforced elastomers are idealized here as 2D solids comprised of a periodic distribution of long aligned nonlinear elastic fibers that are bonded to a nonlinear elastic matrix phase through interphases, as detailed in Section 2. By means of homogenization and Floquet analyses of the relevant equations of elastostatics, we then generate solutions for the macroscopic response — in Section 3 — and onset of instabilities — in Sections 4 and 5 — for this class of reinforced materials directly in terms of the size and behavior of the interphases. Representative numerical results are presented and discussed in Section 6 followed by some concluding remarks in Section 7.

Email addresses: bertoldi@seas.harvard.edu (Katia Bertoldi), pamies@illinois.edu (Oscar Lopez-Pamies)

2. Problem formulation

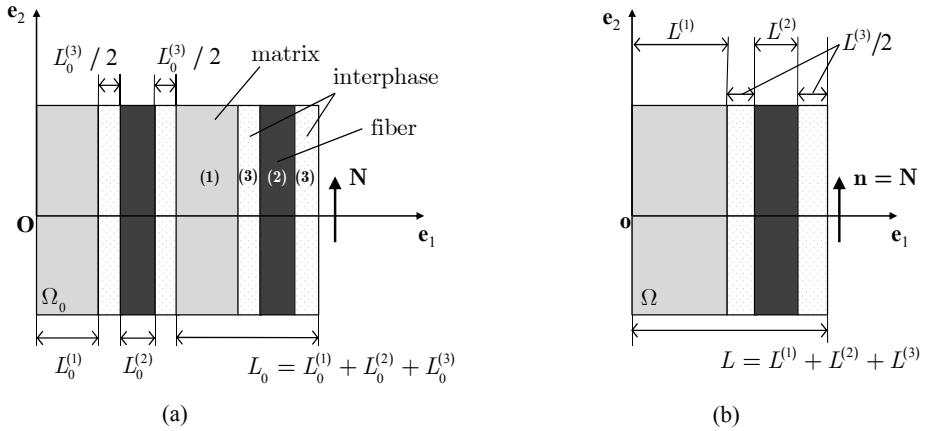

Figure 1: (a) Schematic of two unit cells (or repeat lengths) of a fiber-reinforced elastomer with interphases in the undeformed configuration Ω_0. Materials $r = 1, 2, 3$ characterize the matrix, fibers, and interphases, respectively. The initial fiber direction and repeat length are denoted by $\mathbf{N}$ and L_0. (b) Unit cell in the deformed configuration Ω of the axially stretched fiber-reinforced elastomer before the occurrence of an instability.

Since 2D idealizations of fiber-reinforced materials — utilized by Rosen [10] and later formalized by Triantafyllidis and Maker [11] in their classical works — are known to lead to results that are qualitatively similar to their 3D counterparts [12, 13], here we consider a 2D periodic distribution of long aligned fibers that are bonded to a matrix phase through interphases. Thus we focus on fiber-reinforced elastomers made up of layers of three different materials ($r = 1, 2, 3$), with volume fractions $c_0^{(r)} = L_0^{(r)}/L_0$ in the undeformed stress-free configuration Ω_0, that are periodically intercalated in the sequence shown in Fig. 1(a). Material $r = 1$ corresponds to the matrix phase, whereas materials $r = 2$ and $r = 3$ correspond to the fibers and interphases, respectively. The domains occupied by each individual phase are denoted by $\Omega_0^{(r)}$ so that $\Omega_0 = \Omega_0^{(1)} \bigcup \Omega_0^{(2)} \bigcup \Omega_0^{(3)}$. The initial fiber direction and repeat length are designated by the unit vector $\mathbf{N}$ and scalar L_0. In the sequel, the *microscopic* size L_0 is assumed to be much smaller than the *macroscopic* size of Ω_0, so that Ω_0 can be regarded as a representative volume element.

Material points in the solid are identified by their initial position vector $\mathbf{X}$ in Ω_0. Upon deformation the position vector of a point in the deformed configuration Ω is specified by $\mathbf{x} = \boldsymbol{\chi}(\mathbf{X})$, where $\boldsymbol{\chi}$ is a continuous and one-to-one mapping from Ω_0 to Ω. The pointwise deformation gradient tensor is denoted by $\mathbf{F} = \mathrm{Grad}\boldsymbol{\chi}$.

All three materials are assumed to be homogenous[1] nonlinear elastic characterized by strongly elliptic stored-energy functions $W^{(r)}$ of $\mathbf{F}$. At each material point $\mathbf{X}$ in the undeformed configuration, the first Piola–Kirchhoff stress $\mathbf{S}$ is thus related to the deformation gradient $\mathbf{F}$ by

$$\mathbf{S} = \frac{\partial W}{\partial \mathbf{F}}(\mathbf{X}, \mathbf{F}), \qquad W(\mathbf{X}, \mathbf{F}) = \sum_{r=1}^{3} \theta_0^{(r)}(\mathbf{X}) W^{(r)}(\mathbf{F}), \tag{1}$$

where the indicator function $\theta_0^{(r)}$ is equal to 1 if the position vector $\mathbf{X}$ is inside phase r and zero otherwise. More specifically, owing to the assumed separation of length scales and the periodicity of the microstructure

$$\theta_0^{(r)}(X_1, X_2) = \theta_0^{(r)}(X_1 + q_1 L_0, X_2 + r_2), \tag{2}$$

where q_1 is an arbitrary integer, r_2 is an arbitrary real number, and the fiber direction $\mathbf{N}$ has been tacitly identified (without loss of generality) with the laboratory Cartesian basis vector $\mathbf{e}_2$ (see Fig. 1(a)).

[1]The development that follows can be easily generalized to interphases that are not homogeneous, such as for instance graded interphases.

The overall or macroscopic constitutive response for the above-described reinforced solid is defined as the relation between the volume averages of the first Piola-Kirchoff stress $\overline{\mathbf{S}} \doteq |\Omega_0|^{-1} \int_{\Omega_0} \mathbf{S}(\mathbf{X}) \mathrm{d}\mathbf{X}$ and the deformation gradient $\overline{\mathbf{F}} \doteq |\Omega_0|^{-1} \int_{\Omega_0} \mathbf{F}(\mathbf{X}) \mathrm{d}\mathbf{X}$ over Ω_0 under affine displacement boundary conditions [14, 15]. The result reads formally as

$$\overline{\mathbf{S}} = \frac{\partial \overline{W}}{\partial \overline{\mathbf{F}}}(\overline{\mathbf{F}}), \qquad \overline{W}(\overline{\mathbf{F}}) = \min_{\mathbf{F} \in \mathcal{K}(\overline{\mathbf{F}})} \frac{1}{|\Omega_0|} \int_{\Omega_0} W(\mathbf{X}, \mathbf{F}) \mathrm{d}\mathbf{X}, \tag{3}$$

where $\mathcal{K}$ denotes a suitably defined set of admissible deformations [16, 17]. $\overline{W}$ is the so-called effective stored-energy function and represents physically the total elastic energy (per unit undeformed volume) stored in the material. For small macroscopic deformations (near $\overline{\mathbf{F}} = \mathbf{I}$) the minimization in $(3)_2$ is expected to yield a well-posed linearly elastic problem with a unique solution. As $\overline{\mathbf{F}}$ deviates from $\mathbf{I}$ beyond the linearly elastic neighborhood into the finite-deformation regime, the minimization in $(3)_2$ may yield, however, more than one equilibrium solution with different overall energies. Physically such a bifurcation signals the possible development of an instability.

Following the work of Triantafyllidis and collaborators (see, e.g., [11, 18, 19]), it is useful to make the distinction between "microscopic" instabilities, that is, instabilities with wavelengths that are of the order of the size of the microstructure L_0, and "macroscopic" instabilities, that is, instabilities with much larger wavelengths comparable to the size of Ω_0. The computation of microscopic instabilities is in general a difficult task, though, for the class of 2D fiber-reinforced materials of interest in this work, they can be computed elegantly by making use of Floquet theory [11, 19]. On the other hand, the computation of macroscopic instabilities is a much simpler task, since it reduces to the detection of loss of strong ellipticity of the effective stored-energy function $\overline{W}$ [18].

The aim of this paper is to gain insight into the effect that interphases can have — via their relative size $c_0^{(3)}$ and constitutive behavior $W^{(3)}$ — on the macroscopic response and onset of instabilities in fiber-reinforced elastomers, as characterized by (3). In the sequel, for definiteness, we will focus on a specific choice of energies $W^{(r)}$ for the matrix, fibers, and interphases that are general enough to contain all the essentials of the problem and that at the same time lead to analytical solutions. The analysis of the macroscopic response is presented in the next section, while the computations of the microscopic and macroscopic instabilities are the focus of Sections 4 and 5.

3. Macroscopic response of a fiber-reinforced Neo-Hookean material with interphases

While the formulation presented in the previous section applies to nonlinear elastic materials characterized by arbitrary stored-energy functions $W^{(r)}$, in this section and subsequently we consider the matrix ($r = 1$) and the fibers ($r = 2$) to be *incompressible* and isotropic nonlinear elastic solids characterized by Neo-Hookean stored-energy functions of the form

$$W^{(r)}(\mathbf{F}) = \begin{cases} \dfrac{\mu^{(r)}}{2} (\mathbf{F} \cdot \mathbf{F} - 2) & \text{if} \quad \det \mathbf{F} = 1, \\ +\infty & \text{otherwise.} \end{cases} \tag{4}$$

On the other hand, the interphases are assumed to be characterized by the *compressible* Neo-Hookean stored-energy function

$$W^{(3)}(\mathbf{F}) = \frac{\mu^{(3)}}{2} (\mathbf{F} \cdot \mathbf{F} - 2) + h(J), \tag{5}$$

where the material parameters $\mu^{(r)} > 0$ denote the shear moduli of the three different constituents at zero strain and h is an arbitrary convex[2] function of $J \doteq \det \mathbf{F}$ that satisfies the linearization conditions $h(1) = 0$ and $h'(1) \doteq \mathrm{d}h(1)/\mathrm{d}J = -\mu^{(3)}$. A particular example that will be utilized later in the results section is given by

$$h(J) = \mu^{(3)}[J \ln J + 2(1 - J)] + k \left[\frac{1}{m+1} - \frac{J(-J^m + m + 1)}{m(m+1)} \right], \tag{6}$$

[2]Here, h is required to be convex in order to automatically ensure strong ellipticity of $W^{(3)}$.

where $k > 0$ and $m < 0$ are material constants. Comments on the constitutive choice (5) with (6) for the interphases are deferred to Section 6.

3.1. Local deformation and stress fields at equilibrium

Having specified the constitutive behaviors (4)–(5) for the matrix, fibers, and interphases, we next turn to computing the pointwise deformation gradient field $\mathbf{F}(\mathbf{X})$ that minimizes the functional $(3)_2$, from which we will then be able to compute the macroscopic constitutive relation between $\overline{\mathbf{S}}$ and $\overline{\mathbf{F}}$. Similar to the corresponding case in linear elasticity (see, e.g., Chapter 9 in [20]), the equilibrium solution $\mathbf{F}(\mathbf{X})$ to the nonlinear problem $(3)_2$ can be shown to be *uniform per phase* up to the onset of a first instability [21]. When specialized to the stored-energy functions (4)–(5), such a solution can in turn be computed in *closed form*. The result reads as

$$\mathbf{F}(\mathbf{X}) = \begin{cases} \overline{\mathbf{F}}^{(1)} = \overline{\mathbf{F}} + \boldsymbol{\alpha} \otimes \mathbf{N}^{\perp} & \text{if} \quad \mathbf{X} \in \Omega_0^{(1)} \\ \overline{\mathbf{F}}^{(2)} = \overline{\mathbf{F}} + \boldsymbol{\beta} \otimes \mathbf{N}^{\perp} & \text{if} \quad \mathbf{X} \in \Omega_0^{(2)} \\ \overline{\mathbf{F}}^{(3)} = \overline{\mathbf{F}} + \boldsymbol{\gamma} \otimes \mathbf{N}^{\perp} & \text{if} \quad \mathbf{X} \in \Omega_0^{(3)} \end{cases}, \tag{7}$$

where the unit vector $\mathbf{N}^{\perp}$ is defined via $\mathbf{N}^{\perp} \cdot \mathbf{N} = 0$,

$$\begin{aligned} \boldsymbol{\alpha} &= \delta\, \overline{\mathbf{F}}\mathbf{N}^{\perp} + \frac{1-(1+\delta)\overline{J}}{\overline{\mathbf{F}}\mathbf{N}\cdot\overline{\mathbf{F}}\mathbf{N}}\, \overline{J}\, \overline{\mathbf{F}}^{-T}\mathbf{N}^{\perp}, \\ \boldsymbol{\beta} &= -\frac{\mu^{(2)} - (1+\delta)\mu^{(1)}}{\mu^{(2)}}\, \overline{\mathbf{F}}\mathbf{N}^{\perp} + \frac{\mu^{(2)} - (1+\delta)\mu^{(1)}\overline{J}}{\mu^{(2)}\overline{\mathbf{F}}\mathbf{N}\cdot\overline{\mathbf{F}}\mathbf{N}}\, \overline{J}\, \overline{\mathbf{F}}^{-T}\mathbf{N}^{\perp}, \\ \boldsymbol{\gamma} &= -\frac{c_0^{(1)}}{c_0^{(3)}}\boldsymbol{\alpha} - \frac{c_0^{(2)}}{c_0^{(3)}}\boldsymbol{\beta} \end{aligned} \tag{8}$$

with

$$\delta = \frac{c_0^{(2)}(\mu^{(2)} - \mu^{(1)})\mu^{(3)} + c_0^{(3)}(\mu^{(3)} - \mu^{(1)})\mu^{(2)}}{c_0^{(1)}\mu^{(2)}\mu^{(3)} + c_0^{(2)}\mu^{(1)}\mu^{(3)} + c_0^{(3)}\mu^{(1)}\mu^{(2)}}, \tag{9}$$

and $\overline{J} \doteq \det \overline{\mathbf{F}}$. Owing to the incompressibility of the matrix and fibers, the macroscopic deformation gradient $\overline{\mathbf{F}}$ in (7) must satisfy the unilateral constraint

$$\overline{J}^{(3)} \doteq \det \overline{\mathbf{F}}^{(3)} = \frac{\overline{J} - 1 + c_0^{(3)}}{c_0^{(3)}} > 0, \tag{10}$$

so that material impenetrability is not violated. It is also noteworthy that the field $\mathbf{F}(\mathbf{X})$ turns out to be independent of the function $h(J)$, which serves to characterize the compressibility of the interphasial material, because of the incompressibility of the matrix and fibers.

Up to the onset of a first instability, the resulting local stress field $\mathbf{S}(\mathbf{X})$ at equilibrium is of course also *uniform per phase* and can be simply written as

$$\mathbf{S}(\mathbf{X}) = \begin{cases} \overline{\mathbf{S}}^{(1)} = \mu^{(1)}(\overline{\mathbf{F}} + \boldsymbol{\alpha} \otimes \mathbf{N}^{\perp}) - p^{(1)} \left(\overline{\mathbf{F}}^{-T} - \overline{J}\, \overline{\mathbf{F}}^{-T}\mathbf{N}^{\perp} \otimes \overline{\mathbf{F}}^{-1}\boldsymbol{\alpha} \right) & \text{if} \quad \mathbf{X} \in \Omega_0^{(1)} \\ \overline{\mathbf{S}}^{(2)} = \mu^{(2)}(\overline{\mathbf{F}} + \boldsymbol{\beta} \otimes \mathbf{N}^{\perp}) - p^{(2)} \left(\overline{\mathbf{F}}^{-T} - \overline{J}\, \overline{\mathbf{F}}^{-T}\mathbf{N}^{\perp} \otimes \overline{\mathbf{F}}^{-1}\boldsymbol{\beta} \right) & \text{if} \quad \mathbf{X} \in \Omega_0^{(2)} \\ \overline{\mathbf{S}}^{(3)} = \mu^{(3)} \left(\overline{\mathbf{F}} + \boldsymbol{\gamma} \otimes \mathbf{N}^{\perp} \right) + h'(\overline{J}^{(3)}) \left(\overline{J}^{(3)} \overline{\mathbf{F}}^{-T} - \overline{J}\, \overline{\mathbf{F}}^{-T}\mathbf{N}^{\perp} \otimes \overline{\mathbf{F}}^{-1}\boldsymbol{\gamma} \right) & \text{if} \quad \mathbf{X} \in \Omega_0^{(3)} \end{cases}, \tag{11}$$

where the vectors $\boldsymbol{\alpha}$, $\boldsymbol{\beta}$, $\boldsymbol{\gamma}$ are given by expressions (8) and

$$\begin{aligned} p^{(1)} &= \frac{\overline{J}}{\overline{\mathbf{F}}\mathbf{N}\cdot\overline{\mathbf{F}}\mathbf{N}} \left[\mu^{(1)} - \mu^{(3)} + \left(\mu^{(1)} + \frac{c_0^{(1)} + c_0^{(2)}}{c_0^{(3)}}\mu^{(3)} \right) \frac{1-\overline{J}}{\overline{J}} \right] - h'(\overline{J}^{(3)}), \\ p^{(2)} &= \frac{\overline{J}}{\overline{\mathbf{F}}\mathbf{N}\cdot\overline{\mathbf{F}}\mathbf{N}} \left[\mu^{(2)} - \mu^{(3)} + \left(\mu^{(2)} + \frac{c_0^{(1)} + c_0^{(2)}}{c_0^{(3)}}\mu^{(3)} \right) \frac{1-\overline{J}}{\overline{J}} \right] - h'(\overline{J}^{(3)}). \end{aligned} \tag{12}$$

In contrast to the local deformation (7), note that the local stress field (11) does depend on the compressibility function $h(J)$.

3.2. Macroscopic response

In view of the *explicit* results (7) and (11) for the local fields, it is now a simple matter to compute the macroscopic constitutive response (3) for the above-defined fiber-reinforced Neo-Hookean material with interphases. After some algebraic manipulation, the effective stored-energy function $\overline{W}$ in this case can be shown to take the *closed form*

$$\begin{aligned}\overline{W}(\overline{\mathbf{F}}) &= \sum_{r=1}^{3} c_0^{(r)} W^{(r)}(\overline{\mathbf{F}}^{(r)}) \\ &= \frac{\overline{\mu}_{_V}}{2}\left(\overline{\mathbf{F}}\cdot\overline{\mathbf{F}}-2\right) - \frac{\overline{\mu}_{_V}-\overline{\mu}_{_R}}{2}\,\overline{J}^{\,2}\overline{\mathbf{F}}^{\,-T}\mathbf{N}\cdot\overline{\mathbf{F}}^{\,-T}\mathbf{N} + \\ &\quad \frac{\overline{\mu}_{_V}-\overline{\mu}_{_R}\overline{J}^{\,2}+\mu^{(3)}(\overline{J}-1)(\overline{J}^{(3)}+1)}{2\overline{\mathbf{F}}\mathbf{N}\cdot\overline{\mathbf{F}}\mathbf{N}} + c_0^{(3)} h(\overline{J}^{(3)})\end{aligned} \tag{13}$$

where

$$\overline{\mu}_{_V} = \sum_{r=1}^{3} c_0^{(r)}\mu^{(r)}, \qquad \overline{\mu}_{_R} = \left(\sum_{r=1}^{3}\frac{c_0^{(r)}}{\mu^{(r)}}\right)^{-1}, \tag{14}$$

and it is recalled that $\overline{J}^{(3)}$ is given explicitly by equation (10). The macroscopic stress-deformation relation is in turn given by

$$\begin{aligned}\overline{\mathbf{S}} &= \frac{\partial\overline{W}}{\partial\overline{\mathbf{F}}}(\overline{\mathbf{F}}) = \sum_{r=1}^{3} c_0^{(r)}\overline{\mathbf{S}}^{(r)} \\ &= \overline{\mu}_{_V}\overline{\mathbf{F}} + (\overline{\mu}_{_V}-\overline{\mu}_{_R})\overline{J}^{\,2}\,\overline{\mathbf{F}}^{\,-T}\mathbf{N}\otimes\overline{\mathbf{F}}^{\,-1}\overline{\mathbf{F}}^{\,-T}\mathbf{N} - \\ &\quad \frac{\overline{\mu}_{_V}-\overline{\mu}_{_R}\overline{J}^{\,2}+\mu^{(3)}(\overline{J}-1)(\overline{J}^{(3)}+1)}{(\overline{\mathbf{F}}\mathbf{N}\cdot\overline{\mathbf{F}}\mathbf{N})^{\,2}}\,\overline{\mathbf{F}}\mathbf{N}\otimes\mathbf{N} + \\ &\quad \left[\frac{\left(\mu^{(3)}\overline{J}^{(3)}-\overline{\mu}_{_R}\overline{J}\right)\overline{J}}{\overline{\mathbf{F}}\mathbf{N}\cdot\overline{\mathbf{F}}\mathbf{N}} - (\overline{\mu}_{_V}-\overline{\mu}_{_R})\overline{J}^{\,2}\overline{\mathbf{F}}^{\,-T}\mathbf{N}\cdot\overline{\mathbf{F}}^{\,-T}\mathbf{N} + \overline{J}h'(\overline{J}^{(3)})\right]\overline{\mathbf{F}}^{\,-T}.\end{aligned} \tag{15}$$

A few remarks regarding the above formulae are in order. First we note that the macroscopic constitutive response (15) is transversely isotropic as expected, with the effective stored-energy function (13) depending on the four transversely isotropic invariants $\overline{\mathbf{F}}\cdot\overline{\mathbf{F}}$, $\overline{\mathbf{F}}\mathbf{N}\cdot\overline{\mathbf{F}}\mathbf{N}$, $\overline{\mathbf{F}}^{\,-T}\mathbf{N}\cdot\overline{\mathbf{F}}^{\,-T}\mathbf{N}$, and $\overline{J}$. We note in particular that the dependence on $\overline{J}$, which measures the overall compressibility of the fiber-reinforced solid, is highly non-trivial (and *not* simply additive). The material constants $\mu^{(1)}$, $\mu^{(2)}$ and volume fractions $c_0^{(1)}$, $c_0^{(2)}$ of the matrix and fibers enter the macroscopic relations (13) and (15) simply through the arithmetic $\overline{\mu}_{_V}$ and harmonic $\overline{\mu}_{_R}$ averages (14). On the other hand, the material parameter $\mu^{(3)}$, material function $h(J)$, and volume fraction $c_0^{(3)}$ of the interphases enter (13) and (15) in a more complex manner. For the special case of aligned or axial loading — to be the focus of our analysis subsequently — with

$$\overline{F}_{ij} = \mathrm{diag}(\overline{\lambda}_1, \overline{\lambda}_2), \tag{16}$$

the effective stored-energy function (13) reduces (with a slight abuse of notation) to

$$\overline{W}(\overline{\lambda}_1,\overline{\lambda}_2) = \frac{\overline{\mu}_{_V}}{2}\left(\overline{\lambda}_2^{\,2}+\overline{\lambda}_2^{\,-2}-2\right) - \frac{(1-\overline{\lambda}_1\overline{\lambda}_2)(\overline{\lambda}_1\overline{\lambda}_2-1+2c_0^{(3)})}{2c_0^{(3)}\overline{\lambda}_2^{\,2}}\mu^{(3)} + c_0^{(3)}h(\overline{J}^{(3)}) \tag{17}$$

and the macroscopic stress (15) to $\overline{S}_{ij} = \mathrm{diag}(\bar{t}_1, \bar{t}_2)$ with

$$\begin{aligned}\bar{t}_1 &= \frac{\partial\overline{W}}{\partial\overline{\lambda}_1}(\overline{\lambda}_1,\overline{\lambda}_2) = \frac{\overline{\lambda}_1\overline{\lambda}_2-1+c_0^{(3)}}{c_0^{(3)}\overline{\lambda}_2}\mu^{(3)} + \overline{\lambda}_2 h'(\overline{J}^{(3)}), \\ \bar{t}_2 &= \frac{\partial\overline{W}}{\partial\overline{\lambda}_2}(\overline{\lambda}_1,\overline{\lambda}_2) = \overline{\mu}_{_V}\left(\overline{\lambda}_2-\overline{\lambda}_2^{\,-3}\right) + \frac{\overline{\lambda}_1\overline{\lambda}_2-1+c_0^{(3)}(2-\overline{\lambda}_1\overline{\lambda}_2)}{c_0^{(3)}\overline{\lambda}_2^{\,3}}\mu^{(3)} + \overline{\lambda}_1 h'(\overline{J}^{(3)}),\end{aligned} \tag{18}$$

where now $\overline{J}^{(3)} = (\overline{\lambda}_1\overline{\lambda}_2 - 1 + c_0^{(3)})/c_0^{(3)}$. Finally, it is important to re-emphasize that expressions (13) and (15) may cease to be valid at macroscopic deformations $\overline{\mathbf{F}}$ sufficiently far away from the linearly elastic neighborhood (near $\overline{\mathbf{F}} = \mathbf{I}$) because of the development of instabilities. The computation of the critical deformations $\overline{\mathbf{F}}_{cr}$ and associated critical stresses $\overline{\mathbf{S}}_{cr}$ at which these instabilities first occur along aligned loadings of the form (16) is the subject of the next two sections.

4. Onset of microscopic instabilities

Instabilities in solids are often investigated formulating the relevant incremental boundary value problem in an updated Lagrangian formulation, where the reference configuration moves and is identified with the current configuration (see, e.g., Chapter 6 in [22]). Push-forward transformations allow the introduction of the incremental updated stress quantity $\mathbf{\Sigma}(\mathbf{x})$, so that the incremental equilibrium equation takes the form

$$\operatorname{div} \mathbf{\Sigma} = \mathbf{0}. \tag{19}$$

In the case of nonlinear elastic materials characterized by a stored-energy function $W(\mathbf{X}, \mathbf{F})$, the underlying constitutive equation takes the linear form

$$\mathbf{\Sigma} = \boldsymbol{\mathcal{C}} \operatorname{grad} \mathbf{u} \tag{20}$$

to first order in the incremental deformation field $\mathbf{u}(\mathbf{x}) \doteq \dot{\mathbf{x}}$, where the components of the updated modulus tensor are given by

$$\mathcal{C}_{iqkp} = \frac{1}{J} F_{pl} F_{qj} \frac{\partial^2 W}{\partial F_{ij} \partial F_{kl}}(\mathbf{X}, \mathbf{F}). \tag{21}$$

If, in addition, the material is incompressible, $\mathbf{u}$ must satisfy the constraint $\operatorname{tr}(\operatorname{grad} \mathbf{u}) = 0$ and as a result relation (20) specializes to

$$\mathbf{\Sigma} = \boldsymbol{\mathcal{C}} \operatorname{grad} \mathbf{u} + p \, (\operatorname{grad} \mathbf{u})^T - \dot{p} \, \mathbf{I}, \tag{22}$$

where p and $\dot{p}$ stand for the Lagrange multipliers associated with the incompressibility constraint.

In order to apply the above formalism to the problem of interest here, we begin by recognizing from the periodicity of the microstructure that it suffices to consider equation (19) on just one unit cell of the material — and *not* on the entire domain Ω — together with some additional boundary conditions provided by Floquet theory. Given that our primary focus is on aligned macroscopic loadings (16), we consider the unit cell depicted in Fig. 1(b). Note that, because of the updated Lagrangian formulation, the unit cell is in the deformed configuration Ω and hence the lengths of the axially stretched layers are given by

$$\begin{aligned} L^{(1)} &= \overline{\mathbf{F}}_{11}^{(1)} L_0^{(1)} = \overline{\lambda}_2^{-1} L_0^{(1)}, \\ L^{(2)} &= \overline{\mathbf{F}}_{11}^{(2)} L_0^{(2)} = \overline{\lambda}_2^{-1} L_0^{(2)}, \\ L^{(3)} &= \overline{\mathbf{F}}_{11}^{(3)} L_0^{(3)} = \frac{\overline{\lambda}_1\overline{\lambda}_2 - 1 + c_0^{(3)}}{\overline{\lambda}_2 c_0^{(3)}} L_0^{(3)}, \end{aligned} \tag{23}$$

as dictated by the underlying local deformation gradient (7). Because the underlying microstructure is *piecewise homogeneous*, note further that continuity of the incremental deformation $\mathbf{u}$ and traction $\mathbf{\Sigma}\mathbf{n}^{\perp}$ requires that

$$\begin{aligned} &[\![\mathbf{u}(x_1 + L^{(1)}, x_2)]\!] = \mathbf{0}, && [\![\mathbf{\Sigma}(x_1 + L^{(1)}, x_2)]\!]\mathbf{n}^{\perp} = \mathbf{0}, \\ &[\![\mathbf{u}(x_1 + L^{(1)} + L^{(3)}/2, x_2)]\!] = \mathbf{0}, && [\![\mathbf{\Sigma}(x_1 + L^{(1)} + L^{(3)}/2, x_2)]\!]\mathbf{n}^{\perp} = \mathbf{0}, \\ &[\![\mathbf{u}(x_1 + L^{(1)} + L^{(3)}/2 + L^{(2)}, x_2)]\!] = \mathbf{0}, && [\![\mathbf{\Sigma}(x_1 + L^{(1)} + L^{(3)}/2 + L^{(2)}, x_2)]\!]\mathbf{n}^{\perp} = \mathbf{0}, \\ &[\![\mathbf{u}(x_1 + L, x_2)]\!] = \mathbf{0}, && [\![\mathbf{\Sigma}(x_1 + L, x_2)]\!]\mathbf{n}^{\perp} = \mathbf{0}, \end{aligned} \tag{24}$$

where $\mathbf{n}^{\perp} = \mathbf{N}^{\perp}$ (since under loadings (16) the fibers do not rotate) and the notation $[\![f]\!]$ has been introduced to denote the difference in the values of any field quantity f when evaluated on both sides of an interface.

Matrix and fibers. Having identified the unit cell on which to carry out the incremental analysis, our next step is to seek solutions to (19) of the form

$$\mathbf{u}^{(r)}(x_1,\,x_2)=\mathbf{v}^{(r)}(x_1)\exp[\mathrm{i}\,k_2\,x_2],\quad \dot{p}^{(r)}(x_1,\,x_2)=q^{(r)}(x_1)\exp[\mathrm{i}\,k_2\,x_2],\qquad k_2\in(0,+\infty) \tag{25}$$

for the *incompressible* matrix material $r=1$ and fibers $r=2$. The incompressibility constraint requires that

$$\mathrm{i}\,k_2\,v_2^{(r)}+(v_1^{(r)})'=0, \tag{26}$$

where the dependency of $\mathbf{v}$ on x_1 has been omitted for notational simplicity and $(\,\cdot\,)'\doteq \mathrm{d}(\,\cdot\,)/\mathrm{d}x_1$. Substituting expressions (25)–(26) into the incremental equilibrium equation (19), and making use of the notation $\mathcal{C}^{(r)}_{iqkp}=\frac{1}{\det\overline{\mathbf{F}}^{(r)}}\overline{F}^{(r)}_{pl}\overline{F}^{(r)}_{qj}\partial^2 W^{(r)}(\overline{\mathbf{F}}^{(r)})/\partial F_{ij}\partial F_{kl}$, leads to the following system of linear ordinary differential equations

$$\begin{aligned}&(q^{(r)})'+k_2^2\mathcal{C}^{(r)}_{1212}v_1^{(r)}+\mathrm{i}k_2\left(\mathcal{C}^{(r)}_{1111}-\mathcal{C}^{(r)}_{1122}-\mathcal{C}^{(r)}_{1221}\right)(v_2^{(r)})'=0\\&\mathcal{C}^{(r)}_{2121}(v_2^{(r)})''+k_2^2(\mathcal{C}^{(r)}_{1122}+\mathcal{C}^{(r)}_{1221}-\mathcal{C}^{(r)}_{2222})v_2^{(r)}-\mathrm{i}\,k_2\,q^{(r)}=0\end{aligned} \tag{27}$$

for the unknowns $v_1^{(r)}, v_2^{(r)}$, and $q^{(r)}$ in each phase $r=1,2$. By defining the 4×4 matrix $\mathbf{V}^{(r)}$ with non-zero entries

$$\begin{aligned}&V_{12}^{(r)}=-\mathrm{i}\,k_2,\quad V_{23}=1,\quad V_{32}=-k_2^2\frac{\mathcal{C}^{(r)}_{1122}+\mathcal{C}^{(r)}_{1221}-\mathcal{C}^{(r)}_{2222}}{\mathcal{C}^{(r)}_{2121}},\quad V_{34}^{(r)}=\mathrm{i}\,k_2\frac{1}{\mathcal{C}^{(r)}_{2121}},\\&V_{41}^{(r)}=-k_2^2\mathcal{C}^{(r)}_{1212},\qquad V_{43}^{(r)}=-\mathrm{i}k_2\left(\mathcal{C}^{(r)}_{1111}-\mathcal{C}^{(r)}_{1122}-\mathcal{C}^{(r)}_{1221}\right),\end{aligned} \tag{28}$$

the solution to (27) can be compactly written as

$$\mathbf{y}^{(r)}(x_1)=\mathbf{W}^{(r)}\,\exp[\,\mathbf{Z}^{(r)}x_2]\,\mathbf{a}^{(r)}, \tag{29}$$

where $\mathbf{y}^{(r)}=[v_1^{(r)}\quad v_2^{(r)}\quad (v_2^{(r)})'\quad q^{(r)}]^T$. Here, $\mathbf{Z}^{(r)}$ and $\mathbf{W}^{(r)}$ are 4×4 matrices defined as $\mathbf{Z}^{(r)}=\mathrm{diag}(z_1^{(r)},z_2^{(r)},z_3^{(r)},z_4^{(r)})$ and $\mathbf{W}^{(r)}=[\mathbf{w}_1^{(r)}|\mathbf{w}_2^{(r)}|\mathbf{w}_3^{(r)}|\mathbf{w}_4^{(r)}]$ with $z_I^{(r)}$ and $\mathbf{w}_I^{(r)}$ $(I=1,2,3,4)$ denoting the eigenvalues and corresponding eigenvectors of the matrix $\mathbf{V}^{(r)}$, while $\mathbf{a}^{(r)}$ is a vector of unknown constants.

Interphases. In turn, for the *compressible* interphases ($r=3$), we seek solutions of the form

$$\mathbf{u}^{(3)}(x_1,\,x_2)=\mathbf{v}^{(3)}(x_1)\exp[\mathrm{i}\,k_2\,x_2]. \tag{30}$$

Upon substitution of expression (30) in (19) the following system of ordinary differential equations is generated

$$\begin{aligned}&\mathcal{C}^{(3)}_{1111}(v_1^{(3)})''-k_2^2\mathcal{C}^{(3)}_{1212}v_1^{(3)}+\mathrm{i}\,k_2\left(\mathcal{C}^{(3)}_{1122}+\mathcal{C}^{(3)}_{1221}\right)(v_2^{(3)})'=0\\&\mathcal{C}^{(3)}_{2121}(v_2^{(3)})''-k_2^2\mathcal{C}^{(3)}_{2222}v_2^{(3)}+\mathrm{i}\,k_2\left(\mathcal{C}^{(3)}_{1122}+\mathcal{C}^{(3)}_{1221}\right)(v_1^{(3)})'=0\end{aligned} \tag{31}$$

for $v_1^{(3)}$ and $v_2^{(3)}$. Similar to the previous case, by introducing the 4×4 matrix $\mathbf{V}^{(3)}$ with non-zero entries

$$\begin{aligned}&V_{13}^{(3)}=V_{24}^{(3)}=1,\quad V_{31}^{(3)}=k_2^2\frac{\mathcal{C}^{(3)}_{1212}}{\mathcal{C}^{(3)}_{1111}},\quad V_{34}^{(3)}=-\mathrm{i}\,k_2\,\frac{\mathcal{C}^{(3)}_{1122}+\mathcal{C}^{(3)}_{1221}}{\mathcal{C}^{(3)}_{1111}},\\&V_{42}^{(3)}=k_2^2\frac{\mathcal{C}^{(3)}_{2222}}{\mathcal{C}^{(3)}_{2121}},\quad V_{43}^{(3)}=-\mathrm{i}\,k_2\frac{\mathcal{C}^{(3)}_{1122}+\mathcal{C}^{(3)}_{1221}}{\mathcal{C}^{(3)}_{2121}},\end{aligned} \tag{32}$$

the solution to (31) can be expediently written as

$$\mathbf{y}^{(3)}(x_1)=\begin{cases}\mathbf{W}^{(3)}\,\exp[\,\mathbf{Z}^{(3)}x_2]\,\mathbf{a}^{(3)} & \text{if}\quad x_1\in[L^{(1)},L^{(1)}+L^{(3)}/2]\\ \mathbf{W}^{(3)}\,\exp[\,\mathbf{Z}^{(3)}x_2]\,\mathbf{b}^{(3)} & \text{if}\quad x_1\in[L^{(1)}+L^{(2)}+L^{(3)}/2,L]\end{cases} \tag{33}$$

where now $\mathbf{y}^{(3)}=[v_1^{(3)}\quad v_2^{(3)}\quad (v_1^{(3)})'\quad (v_2^{(3)})']^T$. In this last expression, $\mathbf{Z}^{(3)}=\mathrm{diag}(z_1^{(3)},z_2^{(3)},z_3^{(3)},z_4^{(3)})$ and $\mathbf{W}^{(3)}=[\mathbf{w}_1^{(3)}|\mathbf{w}_2^{(3)}|\mathbf{w}_3^{(3)}|\mathbf{w}_4^{(3)}]$, where $z_I^{(3)}$ and $\mathbf{w}_I^{(3)}$ $(I=1,2,3,4)$ denote the eigenvalues and corresponding eigenvectors of the matrix $\mathbf{V}^{(3)}$, and $\mathbf{a}^{(3)}$ and $\mathbf{b}^{(3)}$ are vectors of unknown constants.

4.1. Floquet analysis

In view of the periodicity of the microstructure, the solution along the x_1 direction must satisfy the Floquet relation (see, e.g., Chapter 15.7 in [23])

$$\mathbf{y}^{(1)}(x_1 + L) = \mathbf{y}^{(1)}(x_1)\exp[\mathrm{i}k_1 L], \tag{34}$$

where the real number $k_1 \in [0, 2\pi/L)$ is the so-called Floquet parameter of the solution. After substituting expressions (25) and (30) with (29) and (33) in the interface conditions (24) and then making use of the Floquet relation (34), it is not difficult to deduce that a non-trivial solution $\mathbf{u}(\mathbf{x}) \neq \mathbf{0}$ to the incremental problem (19) exists when

$$\det\left[\,\mathbf{K}(\,\overline{\lambda}_1, \overline{\lambda}_2; k_2) - \exp[\mathrm{i}k_1 L]\,\boldsymbol{\mathcal{I}}\,\right] = 0 \tag{35}$$

for some $k_2 \in (0, +\infty)$ and $k_1 \in [0, 2\pi/L)$, where $\boldsymbol{\mathcal{I}}$ denotes the 4×4 identity matrix and $\mathbf{K}$ is given by

$$\begin{aligned}\mathbf{K} = (\mathbf{G}^{(1)})^{-1}\mathbf{G}^{(3)}\exp\left[\mathbf{Z}^{(3)}\frac{L^{(3)}}{2}\right](\mathbf{G}^{(3)})^{-1}\mathbf{G}^{(2)}\exp[\mathbf{Z}^{(2)}L^{(2)}](\mathbf{G}^{(2)})^{-1}\mathbf{G}^{(3)}\exp\left[\mathbf{Z}^{(3)}\frac{L^{(3)}}{2}\right]\\ (\mathbf{G}^{(3)})^{-1}\mathbf{G}^{(1)}\exp[\mathbf{Z}^{(1)}L^{(1)}]\end{aligned} \tag{36}$$

with $\mathbf{G}^{(r)} = \mathbf{Q}^{(r)}\mathbf{W}^{(r)}$, $\mathbf{Q}^{(r)}$ $(r = 1, 2)$ and $\mathbf{Q}^{(3)}$ being 4×4 matrices with the following non-zero entries

$$Q^{(r)}_{11} = Q^{(r)}_{22} = -Q^{(r)}_{34} = 1, \quad Q^{(r)}_{32} = \mathrm{i}\,k_2\left(\mathcal{C}^{(r)}_{1122} - \mathcal{C}^{(r)}_{1111} - p^{(r)}\right), \quad Q^{(r)}_{41} = \mathrm{i}\,k_2\left(\mathcal{C}^{(r)}_{1221} + p^{(r)}\right), \quad Q^{(r)}_{43} = \mathcal{C}^{(r)}_{2121} \tag{37}$$

and

$$Q^{(3)}_{11} = Q^{(3)}_{22} = 1, \qquad Q^{(3)}_{32} = \mathrm{i}k_2\mathcal{C}^{(r)}_{1122}, \qquad Q^{(3)}_{33} = \mathcal{C}^{(3)}_{1111}, \qquad Q^{(3)}_{41} = \mathrm{i}\,k_2\mathcal{C}^{(3)}_{1221}, \qquad Q^{(3)}_{44} = \mathcal{C}^{(3)}_{2121}. \tag{38}$$

Thus, according to equation (35), along an arbitrary diagonal loading path (16) with origin $\overline{\mathbf{F}} = \mathbf{I}$ an instability will first occur in the fiber-reinforced material at the point at which $\Lambda = \exp[\mathrm{i}\,k_1 L]$ becomes an eigenvalue of the matrix $\mathbf{K}$. More explicitly, exploiting the facts that $||\exp[\mathrm{i}\,k_1 L]|| = 1$ and $\det\mathbf{K} = 1$ (since $\sum_{I=1}^{4} z_I^{(r)} = 0$ for $r = 1, 2, 3$ in this case), an instability will first occur at the point at which any of the four conditions

$$A(\overline{\lambda}_1, \overline{\lambda}_2; k_2) \doteq \left|\left|\frac{I_1}{4} + \frac{a(I_1, I_2)}{4} \pm \frac{\sqrt{I_1^2 - 2I_2 - 4 + I_1 a(I_1, I_2)}}{2\sqrt{2}}\right|\right| - 1 = 0, \tag{39}$$

with $a(I_1, I_2) = \pm\sqrt{I_1^2 - 4I_2 + 8}$, $I_1 = \mathrm{tr}\mathbf{K}$, and $I_2 = \left[(\mathrm{tr}\mathbf{K})^2 - \mathrm{tr}\mathbf{K}^2\right]/2$, is satisfied for some positive value of k_2. In addition to the dependency on the size and constitutive behavior of the matrix and fibers, the above derivation explicitly reveals that the onset of instabilities depends as well on the size and constitutive behavior of the interphases — via the matrices $\exp\left[\mathbf{Z}^{(3)}\frac{L^{(3)}}{2}\right]$ and $\mathbf{G}^{(3)}$ in (36). To better reveal this dependency, sample numerical results for the critical deformations and critical stresses at which instabilities occur — as dictated by condition (39) — will be presented in Section 6 and compared with corresponding results for materials without interphases. Before proceeding with these results, it is expedient to discuss in some detail the long wavelength limit $k_2 \to 0$ in (39).

5. Onset of macroscopic instabilities

Long-wavelength or macroscopic instabilities are known to be of particular prominence in fiber-reinforced elastomers [11, 12, 24] and can be detected by taking the limit $k_2 \to 0$ directly in condition (39) and solving the resulting asymptotic problem [11]. Alternatively — as proved by Geymonat et al. [18] in the context of a much more general class of periodic composites — macroscopic instabilities can also be detected from the loss of strong ellipticity of the overall response of the material. Specifically, for the fiber-reinforced materials under study in this work, macroscopic instabilities may develop whenever the condition

$$\min_{||\mathbf{m}||=1} B(\overline{\mathbf{F}}; \mathbf{m}) > 0, \tag{40}$$

with

$$B(\overline{\mathbf{F}};\mathbf{m}) \doteq \det\left[\overline{\mathcal{L}}_{i1k1}\left(\frac{m_1}{m_2}\right)^2 + \left(\overline{\mathcal{L}}_{i1k2}+\overline{\mathcal{L}}_{i2k1}\right)\frac{m_1}{m_2} + \overline{\mathcal{L}}_{i2k2}\right] \quad \text{and} \quad \overline{\boldsymbol{\mathcal{L}}} = \frac{\partial^2 \overline{W}}{\partial\overline{\mathbf{F}}\partial\overline{\mathbf{F}}}(\overline{\mathbf{F}}), \tag{41}$$

is first violated along any arbitrary loading path with starting point $\overline{\mathbf{F}} = \mathbf{I}$.

For aligned loadings of the form (16), it is possible to rewrite condition (40) as a set of three simple and explicit conditions exclusively in terms of the moduli $\overline{\mathcal{L}}_{ijkl}$ [25]. They read as

$$\begin{aligned}
&(i) \qquad \overline{\mathcal{L}}_{1111}\overline{\mathcal{L}}_{2121} > 0,\\
&(ii) \qquad \overline{\mathcal{L}}_{2222}\overline{\mathcal{L}}_{1212} > 0,\\
&(iii) \qquad \sqrt{\overline{\mathcal{L}}_{1111}\overline{\mathcal{L}}_{2121}\overline{\mathcal{L}}_{2222}\overline{\mathcal{L}}_{1212}} + \frac{1}{2}\left[\overline{\mathcal{L}}_{1111}\overline{\mathcal{L}}_{2222} + \overline{\mathcal{L}}_{1212}\overline{\mathcal{L}}_{2121} - (\overline{\mathcal{L}}_{1122}+\overline{\mathcal{L}}_{1221})^2\right] > 0.
\end{aligned} \tag{42}$$

Here, according to $(41)_2$ with (13) and (16),

$$\begin{aligned}
\overline{\mathcal{L}}_{1111} &= \frac{\mu^{(3)} + \overline{\lambda}_2^2 h''(\overline{J}^{(3)})}{c_0^{(3)}},\\
\overline{\mathcal{L}}_{1122} &= \frac{(1-c_0^{(3)})\mu^{(3)} + c_0^{(3)}\overline{\lambda}_2^2 h'(\overline{J}^{(3)}) + \overline{\lambda}_1^2\overline{\lambda}_2^4 h''(\overline{J}^{(3)})}{c_0^{(3)}\overline{\lambda}_2^2},\\
\overline{\mathcal{L}}_{2222} &= \frac{(3-6c_0^{(3)}+2(c_0^{(3)}-1)\overline{\lambda}_1\overline{\lambda}_2)\mu^{(3)} + c_0^{(3)}\overline{\mu}_{_V}(3+\overline{\lambda}_2^4) + \overline{\lambda}_1^2\overline{\lambda}_2^4 h''(\overline{J}^{(3)})}{c_0^{(3)}\overline{\lambda}_2^4},\\
\overline{\mathcal{L}}_{1212} &= \frac{(1-\overline{\lambda}_1\overline{\lambda}_2)(\overline{\lambda}_1\overline{\lambda}_2+2c_0^{(3)}-1)\mu^{(3)} + c_0^{(3)}\overline{\mu}_{_R}\overline{\lambda}_1^2\overline{\lambda}_2^2 + c_0^{(3)}\overline{\mu}_{_V}(\overline{\lambda}_2^4-1)}{c_0^{(3)}\overline{\lambda}_2^4},\\
\overline{\mathcal{L}}_{1221} &= \frac{c_0^{(3)}\overline{\mu}_{_R}\overline{\lambda}_1\overline{\lambda}_2 - (\overline{\lambda}_1\overline{\lambda}_2 - 1 + c_0^{(3)})\mu^{(3)}}{c_0^{(3)}\overline{\lambda}_2^2} - h'(\overline{J}^{(3)}),\\
\overline{\mathcal{L}}_{2121} &= \overline{\mu}_{_R},
\end{aligned} \tag{43}$$

where it is recalled that $\overline{J}^{(3)} = (\overline{\lambda}_1\overline{\lambda}_2 - 1 + c_0^{(3)})/c_0^{(3)}$. Exploring the parameter space for a variety of convex functions $h(J)$ indicates that it is condition (ii) — via $\overline{\mathcal{L}}_{1212} = 0$ — the condition that almost invariably first ceases to hold true. That is, starting at $\overline{\lambda}_1 = \overline{\lambda}_2 = 1$ and marching along loading paths of the form (16), macroscopic instabilities can first develop at stretches $\overline{\lambda}_1$ and $\overline{\lambda}_2$ that satisfy the algebraic condition

$$\mathcal{C}(\overline{\lambda}_1,\overline{\lambda}_2) \doteq \overline{\lambda}_2 - \left[1 - \overline{\lambda}_1^2\overline{\lambda}_2^2\frac{\overline{\mu}_{_R}}{\overline{\mu}_{_V}} + \frac{(\overline{\lambda}_1\overline{\lambda}_2-1)(\overline{\lambda}_1\overline{\lambda}_2+2c_0^{(3)}-1)\mu^{(3)}}{c_0^{(3)}\overline{\mu}_{_V}}\right]^{1/4} = 0. \tag{44}$$

If the material parameters $\mu^{(r)}$ and volume fractions $c_0^{(r)}$ are such that there is no pair of positive real numbers $(\overline{\lambda}_1,\overline{\lambda}_2)$ that satisfies condition (44), macroscopic instabilities do not occur. In the event that macroscopic instabilities do occur, the set of (real and positive) points satisfying condition (44) defines a curve $\mathcal{C}(\overline{\lambda}_1,\overline{\lambda}_2)$ in the $(\overline{\lambda}_1,\overline{\lambda}_2)$–deformation space. Henceforth, we refer to such a curve as *onset-of-macroscopic-instability* curve. The corresponding critical nominal stresses, $\bar{t}_1$ and $\bar{t}_2$, at which macroscopic instabilities occur are given by

$$\begin{aligned}
\bar{t}_1 &= \frac{\partial\overline{W}}{\partial\overline{\lambda}_1}(\overline{\lambda}_1^*,\overline{\lambda}_2^*) = \frac{\overline{\lambda}_1^*\overline{\lambda}_2^* - 1 + c_0^{(3)}}{c_0^{(3)}\overline{\lambda}_2^*}\mu^{(3)} + \overline{\lambda}_2^* h'\left(\frac{\overline{\lambda}_1^*\overline{\lambda}_2^* - 1 + c_0^{(3)}}{c_0^{(3)}}\right),\\
\bar{t}_2 &= \frac{\partial\overline{W}}{\partial\overline{\lambda}_2}(\overline{\lambda}_1^*,\overline{\lambda}_2^*) = \overline{\mu}_{_V}\left(\overline{\lambda}_2^* - \overline{\lambda}_2^{*-3}\right) + \frac{\overline{\lambda}_1^*\overline{\lambda}_2^* - 1 + c_0^{(3)}(2-\overline{\lambda}_1^*\overline{\lambda}_2^*)}{c_0^{(3)}\overline{\lambda}_2^{*3}}\mu^{(3)} + \overline{\lambda}_1^* h'\left(\frac{\overline{\lambda}_1^*\overline{\lambda}_2^* - 1 + c_0^{(3)}}{c_0^{(3)}}\right),
\end{aligned} \tag{45}$$

where, for clarity of notation, $\overline{\lambda}_1^*$ and $\overline{\lambda}_2^*$ have been introduced to denote the critical stretches that satisfy condition (44). The set of points generated by evaluating expressions (45) at all pairs of critical stretches

$(\overline{\lambda}_1^*, \overline{\lambda}_2^*)$ constitutes an onset-of-macroscopic-instability curve $\mathcal{S}(\bar{t}_1, \bar{t}_2)$ in $(\bar{t}_1, \bar{t}_2)$–stress space. Unlike in $(\overline{\lambda}_1, \overline{\lambda}_2)$–deformation space, it is not possible in general to write an explicit formula for $\mathcal{S}(\bar{t}_1, \bar{t}_2)$, but a partial inversion of (45) leads to the semi-explicit expression

$$\mathcal{S}(\bar{t}_1, \bar{t}_2) = \overline{\lambda}_1^* \overline{\lambda}_2^* \left[1 - \overline{\lambda}_1^{*2} \overline{\lambda}_2^{*2} \frac{\overline{\mu}_{_R}}{\overline{\mu}_{_V}} + \frac{(\overline{\lambda}_1^* \overline{\lambda}_2^* - 1)(\overline{\lambda}_1^* \overline{\lambda}_2^* + 2c_0^{(3)} - 1)\mu^{(3)}}{c_0^{(3)} \overline{\mu}_{_V}}\right]^{-1/2} \bar{t}_1 - \bar{t}_2 - \overline{\lambda}_1^{*2} \overline{\lambda}_2^{*2} \overline{\mu}_{_R} \left[1 - \overline{\lambda}_1^{*2} \overline{\lambda}_2^{*2} \frac{\overline{\mu}_{_R}}{\overline{\mu}_{_V}} + \frac{(\overline{\lambda}_1^* \overline{\lambda}_2^* - 1)(\overline{\lambda}_1^* \overline{\lambda}_2^* + 2c_0^{(3)} - 1)\mu^{(3)}}{c_0^{(3)} \overline{\mu}_{_V}}\right]^{-3/4} = 0, \tag{46}$$

which proves helpful for evaluating some limiting cases of practical interest discussed below.

A quick glance at (44) and (46) suffices to recognize that the onset of macroscopic instabilities depends on the size — via $c_0^{(3)}$ — and constitutive behavior — via $\mu^{(3)}$ and $h(J)$ — of the interphases. Such a dependency will be examined with the help of sample numerical results in the next section and compared with corresponding results for materials without interphases. In this connection, it is fitting to remark that the onset-of-macroscopic-instability curves for materials without interphases can be readily computed from (44) and (46) by appropriately taking the limit of vanishingly small volume fraction of interphases $c_0^{(3)} \to 0$ and enforcing the macroscopic incompressibility constraint $\overline{\lambda}_1 \overline{\lambda}_2 = 1$ (resulting from the local incompressibility of the matrix and fibers). The results read as follows

$$\mathcal{C}'(\overline{\lambda}_1 = \overline{\lambda}_2^{-1}, \overline{\lambda}_2) = \mathcal{P}'(\overline{\lambda}_2) = \overline{\lambda}_2 - \left(1 - \frac{\overline{\mu}'_{_R}}{\overline{\mu}'_{_V}}\right)^{1/4} = 0 \tag{47}$$

and

$$\mathcal{S}'(\bar{t}_1, \bar{t}_2) = \left(1 - \frac{\overline{\mu}'_{_R}}{\overline{\mu}'_{_V}}\right)^{-1/2} \bar{t}_1 - \bar{t}_2 - \overline{\mu}'_{_R} \left(1 - \frac{\overline{\mu}'_{_R}}{\overline{\mu}'_{_V}}\right)^{-3/4} = 0. \tag{48}$$

In these last expressions,

$$\overline{\mu}'_{_V} = (1 - c_0^{(2)})\mu^{(1)} + c_0^{(2)} \mu^{(2)} \qquad \text{and} \qquad \overline{\mu}'_{_R} = \left(\frac{1 - c_0^{(2)}}{\mu^{(1)}} + \frac{c_0^{(2)}}{\mu^{(2)}}\right)^{-1} \tag{49}$$

and it is pointed out that the instability curve in deformation space (47) is comprised of just one point because of the incompressibility constraint $\overline{\lambda}_1 \overline{\lambda}_2 = 1$.

5.1. The case of uniaxial compression in the direction of the fibers ($\bar{t}_1 = 0$ and $\overline{\lambda}_2 \leqslant 1$)

For comparison with experiments and with the classical results of Rosen [10] and Triantafyllidis and Maker [11] further below, we now spell out the specialization of conditions (44) and (46) to the case of uniaxial compression in the direction of the fibers, corresponding to $\bar{t}_1 = 0$ and $\overline{\lambda}_2 \leqslant 1$. Under this type of loading condition, it is not difficult to show from (44)–(46) that the critical values $\overline{\lambda}_2^{cr}$ and $\bar{t}_2^{cr}$ of the stretch $\overline{\lambda}_2$ and stress $\bar{t}_2$ at which a macroscopic instability can first develop are given, respectively, by

$$\overline{\lambda}_2^{cr} = \left[1 - z^2 \frac{\overline{\mu}_{_R}}{\overline{\mu}_{_V}} + \frac{(z-1)(z + 2c_0^{(3)} - 1)\mu^{(3)}}{c_0^{(3)} \overline{\mu}_{_V}}\right]^{1/4} \tag{50}$$

and

$$\bar{t}_2^{cr} = -z^2 \overline{\mu}_{_R} \left[1 - z^2 \frac{\overline{\mu}_{_R}}{\overline{\mu}_{_V}} + \frac{(z-1)(z + 2c_0^{(3)} - 1)\mu^{(3)}}{c_0^{(3)} \overline{\mu}_{_V}}\right]^{-3/4}, \tag{51}$$

where z is the real root to the nonlinear algebraic equation

$$\frac{z - 1 + c_0^{(3)}}{c_0^{(3)}} \mu^{(3)} + \left[1 - z^2 \frac{\overline{\mu}_{_R}}{\overline{\mu}_{_V}} + \frac{(z-1)(z + 2c_0^{(3)} - 1)\mu^{(3)}}{c_0^{(3)} \overline{\mu}_{_V}}\right]^{1/2} h'\left(\frac{z - 1 + c_0^{(3)}}{c_0^{(3)}}\right) = 0 \tag{52}$$

closest to 1.

The critical expressions (50) and (51) apply to general heterogeneity contrast $\mu^{(2)}/\mu^{(1)}$ between the matrix and the fibers. In practice, however, actual fibers in reinforced elastomers are usually several orders of magnitude stiffer than the matrix phase. It is hence convenient to record the further simplification of the above result in the limit as $\Delta \doteq 1/\mu^{(2)} \to 0$, when the fibers are taken to be rigid. In this limit, the solution to (52) admits the asymptotic *explicit* form

$$z = 1 - \frac{c_0^{(3)}\mu^{(1)}\mu^{(3)}}{2c_0^{(2)}\left(c_0^{(3)}(\mu^{(1)}-\mu^{(3)})+(1-c_0^{(2)})\mu^{(3)}\right)\left(\mu^{(3)}+h''(1)\right)}\mu^{(3)}\Delta + O(\Delta^2) \tag{53}$$

so that, to first order ($O(\Delta^0)$), the critical stretch (50) and stress (51) reduce to

$$\overline{\lambda}_2^{cr} = 1 \qquad \text{and} \qquad \bar{t}_2^{cr} = -\frac{\mu^{(1)}\mu^{(3)}}{c_0^{(3)}(\mu^{(1)}-\mu^{(3)})+(1-c_0^{(2)})\mu^{(3)}}, \tag{54}$$

irrespectively of the choice of the compressibility function $h(J)$ for the interphases.

5.1.1. Comparison with the classical results of Rosen (1965) and Triantafyllidis and Maker (1985)

In one of the very first works making use of 2D idealizations of fiber-reinforced materials, Rosen [10] considered a material system made up of alternating layers of two different linear elastic isotropic solids that is subjected to uniaxial compressive load along the layers. By means of an energy method, he solved the problem *approximately* and concluded that the critical stretch $\overline{\lambda}_2^{Ros}$ and associated critical stress $\bar{t}_2^{Ros}$ at which macroscopic instabilities develop are given (in the present notation) by

$$\overline{\lambda}_2^{Ros} = 1 - \frac{\mu^{(1)}}{3(1-c_0^{(2)})c_0^{(2)}\mu^{(2)}} \qquad \text{and} \qquad \bar{t}_2^{Ros} = -\frac{\mu^{(1)}}{1-c_0^{(2)}}. \tag{55}$$

Later, Triantafyllidis and Maker [11] re-examined the same 2D idealization within the more general framework of finite elasticity. Specifically, these authors considered alternating layers of two different incompressible Neo-Hookean materials, also under uniaxial compression along the layers. By making use of Floquet theory, they showed that the critical stretch $\overline{\lambda}_2^{TM}$ and associated critical stress $\bar{t}_2^{TM}$ at which macroscopic instabilities can first develop in this case are given (in the present notation) *exactly* by

$$\overline{\lambda}_2^{TM} = \left(1 - \frac{\overline{\mu}'_{_R}}{\overline{\mu}'_{_V}}\right)^{1/4} \qquad \text{and} \qquad \bar{t}_2^{TM} = -\overline{\mu}'_{_R}\left(1 - \frac{\overline{\mu}'_{_R}}{\overline{\mu}'_{_V}}\right)^{-3/4}, \tag{56}$$

where it is recalled that $\overline{\mu}'_{_V}$ and $\overline{\mu}'_{_R}$ are given by expressions (49). While the *approximate* Rosen expressions (55) differ in general from the *exact* results (56), both of these criteria agree identically in the physically relevant limit of rigid fibers, as $\Delta = 1/\mu^{(2)} \to 0$, when they reduce to

$$\overline{\lambda}_2^{Ros} = \overline{\lambda}_2^{TM} = 1 \qquad \text{and} \qquad \bar{t}_2^{Ros} = \bar{t}_2^{TM} = -\frac{\mu^{(1)}}{1-c_0^{(2)}} \tag{57}$$

to first order ($O(\Delta^0)$).

When compared with the classical results (55)–(56), it should be apparent from expressions (50) and (51) that the presence of interphases in fiber-reinforced materials can have a drastic effect on the values of the critical loads at which macroscopic instabilities develop, even for very small volume fraction $c_0^{(3)}$ of interphases. This is more explicitly revealed by the case of rigid fibers, when is easily deduced from relations (54) and (57) that for materials with interphases that are softer than the matrix — in the sense that $\mu^{(3)} < \mu^{(1)}$ and *irrespectively* of the compressibility function $h(J)$ — the onset of macroscopic instabilities can occur at much smaller compressive stresses than for the corresponding materials without interphases. The opposite is true for the case when the interphases are stiffer than the matrix (i.e., $\mu^{(3)} > \mu^{(1)}$). Further comments on this key result are provided in the next section.

6. Sample results and discussion

In this section, the above-derived results for the axial macroscopic response and onset of instabilities in fiber-reinforced materials — as characterized by relations (18), (39), and (44)–(46) — are examined for various values of the underlying geometric and material parameters of the matrix, fibers, and interphases. Prompted by recent experiments[3], all the results that follow correspond to $\mu^{(1)} = 1$, $\mu^{(2)} = 100$, and interphases that are *softer* than the matrix phase so that $\mu^{(3)} < \mu^{(1)}$. For the function $h(J)$ describing the compressibility of the interphases, we make use of expression (6) with $k = 1$ and $m = -2$. This choice corresponds to interphases that are extremely soft under volume increasing deformations, but stiff under volume decreasing ones, similar to the behavior of gaseous substances.

6.1. Macroscopic response

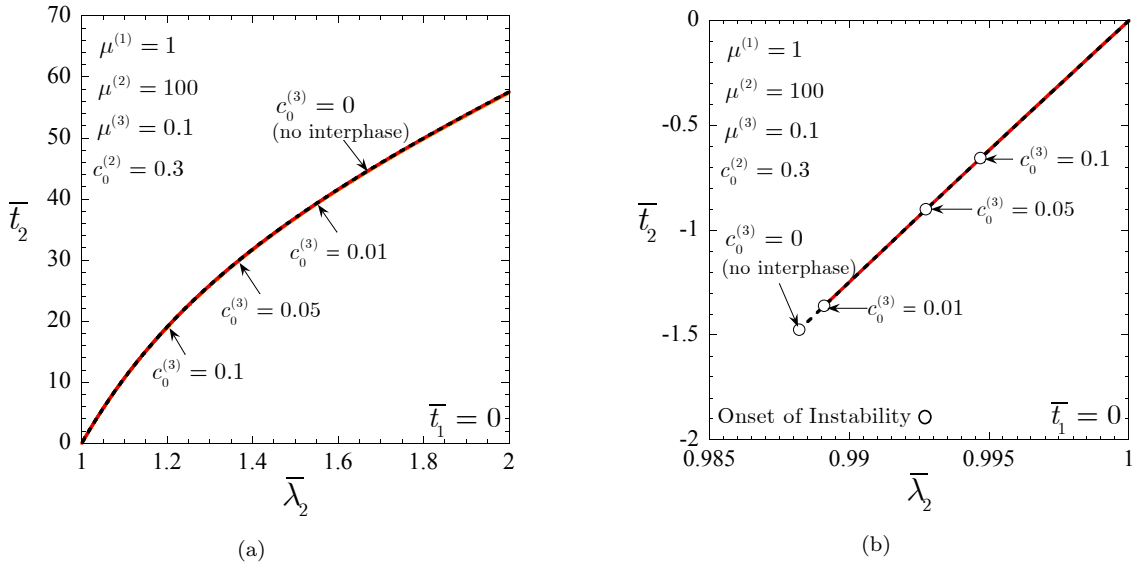

Figure 2: Macroscopic response of fiber-reinforced materials with interphases under uniaxial stress in the fiber direction: $\bar{t}_1 = 0$. The results correspond to $c_0^{(2)} = 30\%$ volume fraction of fibers, interphase shear modulus $\mu^{(3)} = 0.1$, various volume fractions of interphases $c_0^{(3)}$, and are shown in terms of the nominal stress $\bar{t}_2$ as a function of the applied axial stretch $\overline{\lambda}_2$. Part(a) displays the results for tension $\overline{\lambda}_2 \geq 1$, and part (b) for compression $\overline{\lambda}_2 \leq 1$.

Figure 2 shows results for the macroscopic response of fiber-reinforced materials with $c_0^{(2)} = 30\%$ volume fraction of fibers subjected to uniaxial tension — part (a) — and uniaxial compression — part (b) — in the fiber direction (i.e., $\bar{t}_1 = 0$). The results are presented in terms of the nominal stress $\bar{t}_2$ as a function of the applied axial stretch $\overline{\lambda}_2$ for values of interphase shear modulus $\mu^{(3)} = 0.1$ and initial volume fractions $c_0^{(3)} = 0.01, 0.05, 0.1$. The response of the corresponding fiber-reinforced material without interphases ($c_0^{(3)} = 0$) has also been included in the figure (dashed line) for comparison purposes. Note that the plots have been either stopped at the first occurrence of an instability, denoted with the symbol "$\circ$" in the figure, or at some sufficiently large value of the stretch $\overline{\lambda}_2$ if no instability occurs.

A self-evident observation from Fig. 2 is that the presence of interphases does *not* affect the macroscopic (tensile or compressive) uniaxial-stress response of fiber-reinforced materials, as all results agree with that of the material without interphases; although not shown here, varying the values of the interphase shear modulus $\mu^{(3)}$ has been checked not to affect the results either. On the other hand, the presence of

[3]In a recent set of experiments [4], blocks of a transparent elastomer reinforced by cylindrical nitinol rods were axially compressed up to the point at which buckling of the rods was observed. The surfaces of the rods were not treated before fabrication of the composites resulting in fairly weak bonding between the elastomer and the rods.

interphases *does* significantly alter the stability of these material systems under uniaxial compression; no instabilities occur under uniaxial tension. More specifically, the larger the size of the interphases — as measured by their volume fraction $c_0^{(3)}$ here — the less stable the materials become in the sense that instabilities occur at lower values of compressive stresses. Exactly as in the material without interphases, the instabilities in all the materials with interphases ($c_0^{(3)} = 0.01, 0.05, 0.1$) in Fig. 2(b) are of long wavelength.

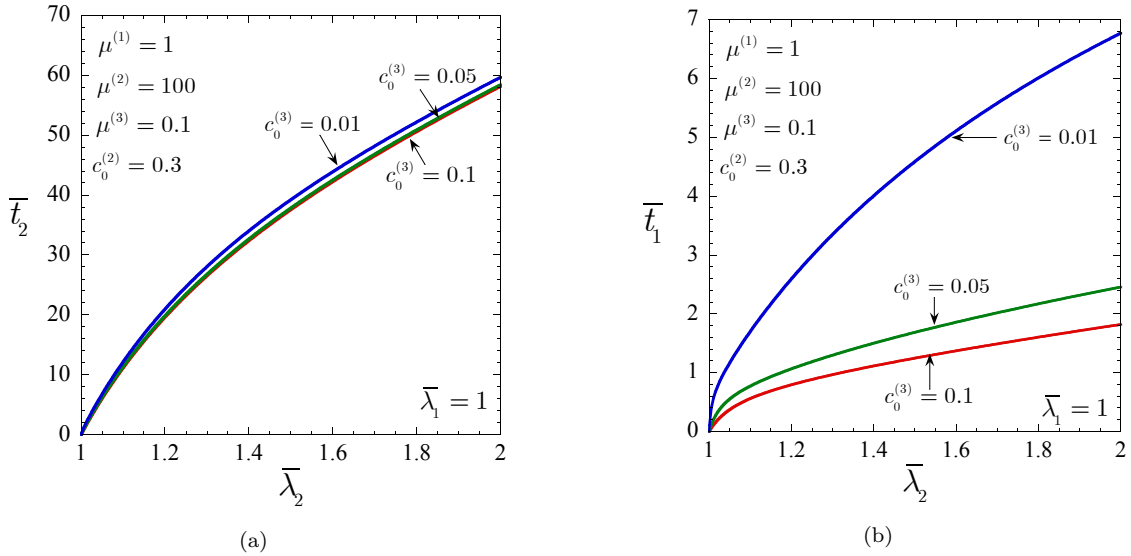

Figure 3: Macroscopic response of fiber-reinforced materials with interphases under uniaxial tensile stretch: $\overline{\lambda}_1 = 1$ and $\overline{\lambda}_2 \geqslant 1$. The results correspond to $c_0^{(2)} = 30\%$ volume fraction of fibers, interphase shear modulus $\mu^{(3)} = 0.1$, and various volume fractions of interphases $c_0^{(3)}$. Part (a) shows results for the nominal stress $\bar{t}_2$ vs. $\overline{\lambda}_2$, whereas part (*b*) shows $\bar{t}_1$ vs. $\overline{\lambda}_2$.

To further probe the axial macroscopic response of fiber-reinforced materials with interphases, Fig. 3 displays results for uniaxial tensile stretch with $\overline{\lambda}_1 = 1$ and $\overline{\lambda}_2 \geq 1$. Plots are shown for $\bar{t}_1$ and $\bar{t}_2$ as functions of $\overline{\lambda}_2$ for the same cases considered in Fig. 2, with the exception that the response of the (incompressible) material without interphases cannot be shown because the imposed loading is not isochoric. Much like for the preceding case of uniaxial stress loading, the stress $\bar{t}_2$ here is seen to be fairly insensitive to the presence of interphases. The stress in the transverse direction $\bar{t}_1$, however, exhibits a stronger dependence on the volume fraction of interphases but this dependency is in actuality negligible when compared to the one-order-of-magnitude larger axial stress $\bar{t}_2$.

In short, the above sample results illustrate that interphases have little influence on the axial macroscopic response of fiber-reinforced materials. This is consistent with the fact that axial loading activates fiber-dominated modes of deformation, and thus the macroscopic response is mostly governed by the behavior of the *stiffer* fibers. By contrast, the above sample results also indicate that interphases can have a strong effect on the development of instabilities. This, in turn, is consistent with the fact that instabilities are controlled by the activation of matrix-dominated (or soft) modes of deformation, and hence the presence of *soft* interphases can have a significant impact on their occurrence. This remarkable effect of interphases on instabilities is examined more thoroughly in the next subsection.

6.2. Onset of instabilities

Figure 4 shows results for the critical stretches $\overline{\lambda}_2^{cr}$ and stresses $\bar{t}_2^{cr}$ at which instabilities develop for the case of uniaxial compressive loading in the fiber direction ($\bar{t}_1 = 0$). The main observation from this figure is that fiber-reinforced materials with thicker (i.e., larger $c_0^{(3)}$) and softer (i.e., smaller $\mu^{(3)}$) interphases are increasingly less stable. In particular, when compared with the material without interphases (dashed line), the critical compressive stretches $\overline{\lambda}_2^{cr}$ and stresses $\bar{t}_2^{cr}$ in materials with interphases can be remarkably lower,

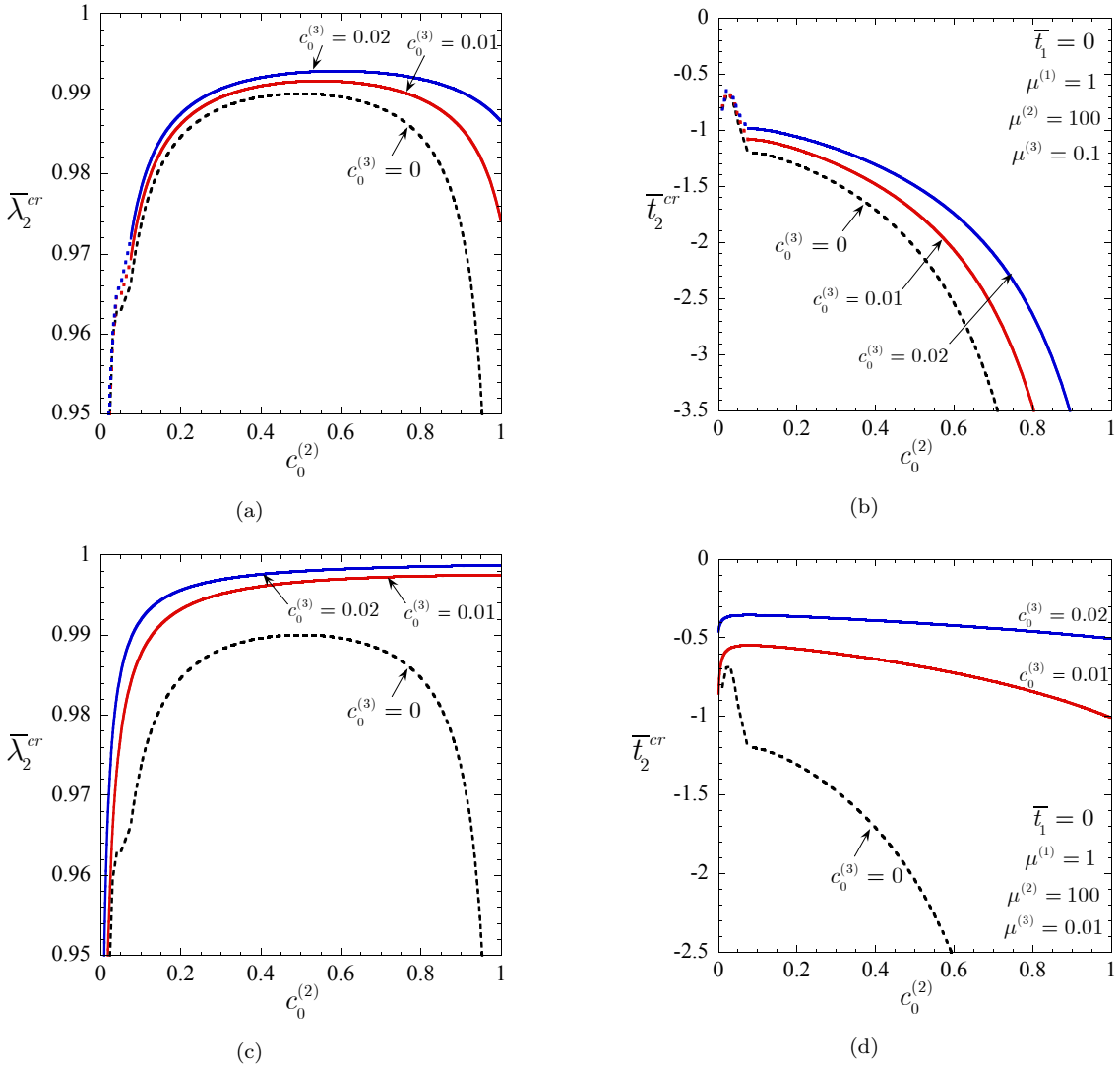

Figure 4: Critical stretches $\overline{\lambda}_2^{cr}$ and stresses $\overline{t}_2^{cr}$ at which instabilities develop in fiber-reinforced materials subjected to uniaxial stress in the fiber direction: $\overline{t}_1 = 0$. The results are shown as functions of the volume fraction of fibers $c_0^{(2)}$ for various values of interphase volume fraction $c_0^{(3)}$ and interphase shear modulus $\mu^{(3)}$.

even for very small volume fraction of interphases in the order of $c_0^{(3)} = 1\%$ or smaller. Another important observation is that all instabilities in Fig. 4 are of long wavelength, except for sufficiently large interphase shear moduli $\mu^{(3)}$ and sufficiently small volume fractions of fibers $c_0^{(2)}$ — greater than $\mu^{(3)} = 0.01$ and less than $c_0^{(2)} = 8\%$ for the cases considered here — when they are of short wavelength. The trend in $c_0^{(2)}$ is similar to that exhibited by instabilities in fiber-reinforced materials without interphases [11]. For clarity, dotted lines are utilized in the plots to indicate that the instabilities are of short wavelength, in contrast to the solid lines utilized to denote long wavelength instabilities.

Onset-of-instability curves for general axial loading are presented in Figure 5. Part (a) shows the curves in $(\overline{\lambda}_1, \overline{\lambda}_2)$–deformation space, while part (b) illustrates them in $(\overline{t}_1, \overline{t}_2)$–stress space. The results correspond to materials with $c_0^{(2)} = 30\%$ volume fraction of fibers, $c_0^{(3)} = 2\%$ of interphases, and interphase shear moduli $\mu^{(3)} = 0.01, 0.05$, and 0.1. For any loading path of choice in both spaces, the first instability that occurs is of long wavelength, as characterized by equations (44) and (46). In deformation space, materials with softer interphases are consistently less stable for small and moderate values of the transverse stretch $\overline{\lambda}_1$. This trend is reversed at sufficiently large stretches $\overline{\lambda}_1 > 1$, when instabilities are seen to develop

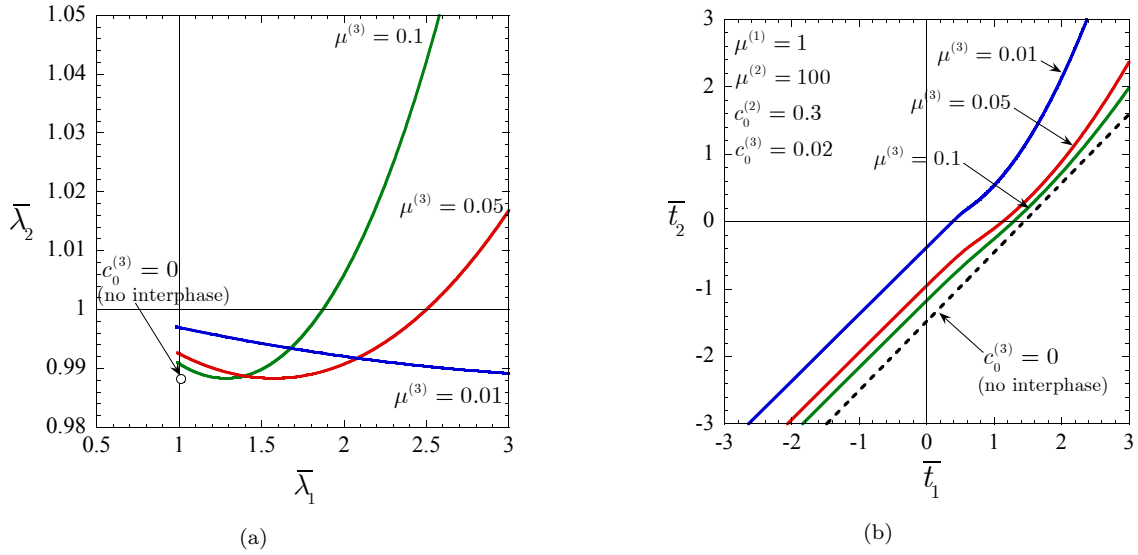

Figure 5: Onset-of-instability curves in $(\overline{\lambda}_1, \overline{\lambda}_2)$–deformation and $(\overline{t}_1, \overline{t}_2)$–stress spaces. The results correspond to materials with $c_0^{(2)} = 30\%$ volume fraction of fibers and $c_0^{(3)} = 2\%$ volume fraction of interphases with shear moduli $\mu^{(3)} = 0.01, 0.05, 0.1$.

not only for compressive but also for *tensile* axial stretches $\overline{\lambda}_2$. In stress space, on the other hand, softer interphases consistently lead to less stable behavior.

7. Final Comments

The results worked out in this paper indicate that while interphases have a marginal effect on the axial macroscopic response of fiber-reinforced elastomers, they can drastically affect their stability. In particular, for the case of materials with interphases that are softer than the matrix, the critical loads at which instabilities develop were found to be significantly lower than in the corresponding materials without interphases, even for very small volume fraction of interphases. At a fundamental level, this behavior can be understood from the fact that instabilities are controlled by the activation of matrix-dominated (or soft) modes of deformation, and hence the presence of soft interphases can have a significant impact on their occurrence.

From a practical point of view, the results also highlight that — in addition to some knowledge of the presence of geometrical and material imperfections [26, 27] — some knowledge of the size and mechanical behavior of the underlying interphases is absolutely necessary in order to be able to accurately predict the compressive failure of fiber-reinforced elastomers.

Finally we remark that it would be interesting to extend the present analysis to non-symmetric loading conditions — where interphases are expected to influence not only the stability but also the macroscopic response — and different geometries of fillers such as for instance spherical particles — where interphasial effects have been reported to play a major role [3, 1, 2].

Acknowledgements

We thank Pedro Reis (Massachusetts Institute of Technology) for sharing with us unpublished experimental data in advance of their publication. OLP acknowledges the National Science Foundation through Grant CMMI–1055528. KB acknowledges the Harvard Materials Research Science and Engineering Center under NSF award number DMR-0820484.

References

[1] Ramier, J., Chazeau, L., Gauthier, C., Guy, L., Bouchereau, M.N., 2007. Influece of silica and its different surface treatments on the vulcanization process of silica filled SBR. *Rubber Chemistry and Technology* 80, 183–193.

[2] Qu, M., Deng, F., Kalkhoran, S.M., Gouldstone, A., Robisson, A., Van Vliet, K.J., 2011. Nanoscale visualization and multiscale mechanical implications of bound rubber interphases in rubber–carbon black nanocomposites. *Soft Matter* 7, 1066–1077.

[3] Ramier, J., 2004. Comportement mécanique d'élastomèrs chargés, influence de l'adhésion charge–polymére, influence de la morphologie. Ph. D. Dissertation, Institut National des Science Appliquées de Lyon, France.

[4] Reis, P., 2011. Buckling of a thin rod embbeded in a soft elastic matrix. Private communication.

[5] Dannenberg, E.M., 1986. Bound rubber and carbon black reinforcement. *Rubber Chem. Technol.* 59, 512–525.

[6] Meissner, B., 1993. Bound rubber theory and experiment. *Journal of Applied Polymer Science* 50, 285–292.

[7] Leblanc, J.L., 2002. Rubber–filler interactions and rheological properties in filled compounds. *Progress in Polymer Science* 27, 627–687.

[8] Walpole, L.J., 1978. A coated inclusion in an elastic medium. *Mathematics Proceedings of the Cambridge Philosophical Society* 83, 495–506.

[9] Hashin, Z., 1991. The spherical inclusion with imperfect interface. *J. Appl. Mech.* 58, 444–449.

[10] Rosen, B.W., 1965. Mechanics of Composite Strengthening. In: Fiber Composite Materials. American Society for Metals 37–75.

[11] Triantafyllidis, N., Maker, B.N., 1985. On the comparison between microscopic and macroscopic instability mechanisms in a class of fiber-reinforced composites. *Journal of Applied Mechanics* 52, 794–800.

[12] Lopez-Pamies, O., Idiart, M.I., 2010. Fiber-reinforced hyperelastic solids: a realizable homogenization constitutive theory. J. *Eng. Math.* 68, 57-83.

[13] Agoras, M., Lopez-Pamies, O., Ponte Castañeda, P., 2009. Onset of macroscopic instabilities in fiber-reinforced nonlinearly elastic materials. *J. Mech. Phys. Solids* 57, 1828–1850.

[14] Hill, R., 1972. On constitutive macrovariables for heterogeneous solids at finite strain. *Proc. R. Soc. Lond. A* 326, 131–147.

[15] Hill, R., Rice, J.R., 1973. Elastic potentials and the structure of inelastic constitutive laws. *SIAM Journal of Applied Mathematics* 25, 448–461.

[16] Braides, A., 1985. Homogenization of some almost periodic coercive functionals. *Rend. Acc. Naz.* XL 9, 313–322.

[17] Müller, S., 1987. Homogenization of nonconvex integral functionals and cellular elastic materials. *Arch. Rat. Mech. Analysis* 99, 189–212.

[18] Geymonat, G., Müller, S., Triantafyllidis, N., 1993. Homogenization of nonlinearly elastic materials, microscopic bifurcation and macroscopic loss of rank-one convexity. *Arch. Rat. Mech. Analysis* 122, 231–290.

[19] Nestorvic, M.D., Triantafyllidis, N., 2004. Onset of failure in finitely strained layered composites subjected to combined normal and shear strain. *J. Mech. Phys. Solids* 52, 941–974.

[20] Milton, G.W., 2002. *The theory of composites*. Cambridge Monographs on Applied and Computational Mathematics, vol. 6. Cambridge University Press, Cambridge.

[21] Lopez-Pamies, O., Ponte Castañeda, P., 2009. Microstructure evolution in hyperelastic laminates and implications for overall behavior and macroscopic stability. *Mechanics of Materials* 41, 364–374.

[22] Ogden, R.W., 1997. *Non-linear elastic deformations*. Dover.

[23] Ince, E.L., 1956. *Ordinary differential equations*. Dover.

[24] Lopez-Pamies, O., Idiart, M., Li, Z., 2011. On microstructure evolution in fiber-reinforced elastomers and implications for their mechanical response and stability. *Journal of Engineering Materials and Technology* 133, 011007.

[25] Hill, R., 1979. On the theory of plane strain in finitely deformed compressible materials. *Math. Proc. Cambridge Philos. Soc.* 86, 161–178.

[26] Jelf, P.M., Fleck, N., 1992. Compression failure mechanisms in unidirectional composites. *Journal of Composite Materials* 26, 2706–2726.

[27] Fleck, N., 1997. Compressive failure of fiber composites. *Advances in Applied Mechanics* 33, 43–117.